JOURNAL OF AIRCRAFT
Vol. 43, No. 2, March–April 2006

Aerodynamic Analysis of a Jet Transport in Windshear Encounter During Landing

Chin-Tang Weng* and Ching-Shun Ho†
National Cheng Kung University, Tainan 701, Taiwan, Republic of China
C. Edward Lan‡
University of Kansas, Lawrence, Kansas 66045
and
Michael Guan§
The Executive Yuan of R.O.C., Taipei 105, Taiwan, Republic of China

Stability and control characteristics of a nominally controllable jet transport airplane that ran off the runway after touchdown during windshear encounter are evaluated based on the data in the onboard flight data recorder (FDR). To determine these characteristics, the recorded wind profile is first improved, and then the unsteady aerodynamic models for the aircraft in dynamic ground effect are estimated. The recorded wind field is improved through the extended-Kalman-filter (EKF) technique to reconstruct the wind profile along the flight path from the data in the FDR. The windshear guideline is reviewed and compared with the airport weather data. To analyze the windshear effect in more detail, unsteady aerodynamic models for the aircraft are developed based on two artificial intelligent methods, the fuzzy-logic modeling and the feed-forward neural networks, applied to the processed FDR data. The stability and control characteristics are then estimated by using these aerodynamic models. The results indicate that a less favorable dynamic ground effect exists near touchdown in crosswind. In addition, the dynamic motion is shown to exhibit directional instability, unstable yaw damping, and loss of control effectiveness near the ground in a combined crab and sideslip landing in unsteady windshear conditions.

Nomenclature

a_x, a_y, a_N	=	longitudinal, lateral, and normal accelerations
b	=	reference wing span
C_x, C_y, C_N, C_l, C_m, C_n	=	aerodynamic forces and moments coefficients
$C_{x_{(\cdot)}}$, $C_{y_{(\cdot)}}$, $C_{N_{(\cdot)}}$, $C_{l_{(\cdot)}}$, $C_{m_{(\cdot)}}$, $C_{n_{(\cdot)}}$	=	nondimensional aerodynamic derivatives
$\bar{c}$	=	mean aerodynamic chord
F, $\bar{F}$	=	F factor and 1-km averaged F factor
k_1	=	longitudinal reduced frequency, $\omega_1 \bar{c}/V$
k_2	=	lateral reduced frequency, $\omega_2 b/2V$
L	=	appropriate length scale for the windshear exposure
N_r	=	number of membership functions
P	=	coefficients of internal functions
p, q, r	=	roll, pitch and yaw rates
R^2	=	square of multiple correlation coefficient
V	=	true airspeed
V_G, $\dot{h}$	=	ground speed and sink rate
V_{w_hor}, ψ_w	=	horizontal wind speed and direction
W_x, W_y, W_z	=	head wind, crosswind, and downdraft
y, $\bar{y}$, $\hat{y}$	=	measured data, average of measured data, and prediction of the fuzzy-logic model
α, β	=	angle of attack and angle of sideslip
δ	=	drift angle
$\delta_{a,e,s,f,r,}$	=	control deflections of aileron, elevator, stabilizer, flap, and rudder
φ, θ, ψ	=	roll, pitch, and yaw angles
ω_1	=	estimated harmonic frequency with the time history of angle of attack
ω_2	=	estimated harmonic frequency with the time history of roll angle

Received 18 January 2005; revision received 8 March 2005; accepted for publication 15 March 2005.

*Assistant Researcher, Satellite Geoinformatics Research Center. Member AIAA.
†Associate Professor, Department of Aeronautics and Astronautics.
‡J. L. Constant Distinguished Professor, Department of Aerospace Engineering. Associate Fellow AIAA.
§Associate Investigator, Aviation Safety Council.

I. Introduction

As generally known, the low-level windshear and turbulence pose a significant hazard to aircraft in the terminal area. In particular, appropriate corrective actions must be applied timely during landing to ensure aircraft safety. To improve flight safety, hazard characterization and acceptable hazard metrics are obviously quite important for pilot situational awareness and accident prevention. U.S. Federal Aviation Administration (FAA) and International Civil Aviation Organization developed windshear guidelines to educate the pilots on the procedures to identify and prevent windshear hazards.[1,2] Based on these guidelines, current Airplane Operations Manual (AOM) and Flight Operation Manual (FOM) all define the hazard threshold[3] in terms of wind speed magnitude. However, studies conducted to determine this threshold were mostly based on aerodynamic models in normal operating conditions. Therefore, the guidelines might not adequately address all hazardous conditions.

To improve these guidelines, identification of windshear/turbulence effects and classification of the hazard level should be emphasized. For this purpose, the National Cheng Kung University research group and Aviation Safety Council (ASC) in Taiwan have cooperated to study 40 flights involving windshear encounters in the takeoff or landing phase. Three current windshear identification methods, the F factor, airspeed variation methods, and the wind variation over unit distance method,[4] have been examined and demonstrated to classify reasonably well the severity of windshear. But none of them is capable of accounting for the crosswind variations and providing adequate warnings to pilots for various aircraft types. It was concluded in Ref. 4 that an aerodynamic analysis would be helpful in analyzing the hazardous level and the stability and

control problems as well. In addition, approach-and-landing accidents, including those involving controlled flight into terrain, loss of control, unstabilized approach, and aircraft icing, also require aerodynamic analysis to verify the unusual physical phenomena. Therefore, for this purpose, a suitable method for aerodynamic analysis is needed.

Traditional approaches of flight data analysis, the stepwise regression and the maximum likelihood being the notable ones, rely on the assumption of quasi-steady aerodynamic models. However, these conventional methods have not been shown to be capable of handling highly nonlinear and unsteady aerodynamic environments possibly exhibited in aircraft accidents, especially in stormy weather conditions. The flexible numerical analysis tools, fuzzy-logic modeling technique (FLM)[5,6] and feed-forward neural networks (FFNNs),[7] should be more suitable for the present application. Because most aerodynamic researchers are more familiar with the FFNN approach, we will use the FFNN approach to verify the FLM results in the present investigation. In Refs. 5, 6, and 8, the FLM was shown to possess an excellent data correlation capability and can establish an accurate model suitable for the problems with uncertainty in measurement data. Pan and Lan[8] also used the FLM algorithm to demonstrate the existence of unstable pitch damping of a jet transport airplane that crashed during a go-around operation with landing flaps and takeoff thrust.

In this paper, the retrieved digital Flight Data Recorder (FDR) from a flight that encountered windshear will be combined with the airport weather forecast data to reconstruct the flight scenario. The FDR data are first analyzed for compatibility with the kinematic equations in airplane flight dynamics, and the force and moment coefficients are then obtained from the flight dynamic equations. Then unsteady, nonlinear aerodynamic models for the airplane will be estimated by using these refined flight data and utilized to analyze the stability and control characteristics.

II. Data Acquisition and Flight Scenario

In this paper, the twin-engine jet airplane in a landing incident on 31 October 2000 at an airport in Taiwan will be considered. The airplane was heading to the Chiang Kai-Shek (CKS) international airport near Taipei for landing.[9] Prior to the incident, a significant weather information on hazardous weather was issued. The CKS weather at the time was poor, having strong wind and heavy rain, because of Xangsane typhoon. However, the visibility was determined to be good enough for an instrument-landing-system approach. Because of a strong crosswind at the final several seconds in flare, the aircraft slipped off the runway after touchdown. The ASC, in its final report[9] on the incident, indicated the causal factors were that the low altitude at the time of autopilot disconnect in relation to the unexpected wind conditions did not allow the pilot sufficient time to gain complete control of the aircraft. The flight crew applied large rudder control to try to decrease the crab angle, but experienced a loss of directional control near the ground.

On the basis of the wind data available to the control tower, as the controller cleared the flight to land the weather conditions were "wind 10 degree, 21 knots, gust 34 knots." The AOM said that the maximum crosswind component for autoland operation was 36 kn on dry runway and reduced by 5 kn on wet and contaminated runways. For landing in low-visibility conditions (CATIII, CAT IIIa) the wind limits of headwind 20 kn, tailwind 10 kn, and crosswind 10 kn shall apply. The maximum demonstrated crosswind limit was 35 kn as indicated in the FOM. Based on these information and guidelines, the aircraft was cleared to land.

In addition, in the terminal area of CKS airport, six sets of anemometers are installed in the middle and at both ends of the runways to monitor the surface wind profile. They measure the wind direction and speed an aircraft will encounter during takeoff and landing and record the mean values every minute. Table 1 shows surface anemometers' 1-min averaged recorded data at the end of 05L (05L in Table 1) and the middle of 05L and 23R (05L/23R in Table 1). It indicated that the wind was varying when the aircraft touched down (TD) at 13:50:12 (UTC). The surface anemometers recorded the wind speed and direction by each minute, which is too coarse for identifying the windshear and analyzing the hazard level. Therefore, the flight data from the FDR are used in this research. After the incident, a low-level wind-shear alert system was installed at the CKS airport in September 2001 to enhance the airport hazard weather forecasting.

Table 1 Anemometers records at airport

UTC time	05L WD, deg/WS, kn[a]	05L Crosswind	05L/23R WD, deg/WS, kn	05L/23R Crosswind
13:47	006/19.2	(L) 13.1[b]	011/23.3	(L) 14.3
13:48	001/16.1	(L) 12.0	001/35.1	(L) 26.1
13:49	351/21.4	(L) 18.1	003/36.0	(L) 25.9
13:50	009/19.3	(L) 12.4	010/35.8	(L) 22.5
13:51	023/19.0	(L) 8.3	008/29.6	(L) 19.4
13:52	005/30.6	(L) 21.3	345/38.5	(L) 34.6

[a]WS, WD presents the wind speed and direction respectively.
[b](L) presents the left wind related 05L landing phase. Touchdown (TD) time was UTC 13:50:12 (+8 h in local time zone).

The jet transport airplane was equipped with many measuring devices to record its responses to various types of input to the system. The available FDR data included, with the sampling rates in parentheses, the longitudinal (4-Hz), lateral (4-Hz), and normal (8-Hz) accelerometer readings (a_x, a_y, a_N), the pitch angles θ (4 Hz), bank angles ϕ (4 Hz), heading angles ψ (1 Hz), ground speeds V_G (1 Hz), drift angles δ (1 Hz), sink rates $\dot{h}$ (1 Hz), angles of attack α (1 Hz), airspeeds V_a (1 Hz), and the control deflections of aileron δ_a (4 Hz), rudder δ_r (4 Hz), elevator δ_e (4 Hz), stabilizer δ_s (1 Hz), and flap δ_f (1 Hz). The recorded data, when necessary, are interpolated with a monotone cubic spline method to result in a set of data with a uniform sampling rate of 4 Hz. The thrust information, that is, the engine tachometer readings, and wind speed and wind direction, are recorded at every 4 s in the FDR. In addition, some variables are not available in the FDR, such as the sideslip angle β and body angular rates p, q, r, and need to be estimated. Therefore, the extended-Kalman-filter (EKF) technique is employed for compatibility check of flight data and estimation of the unmeasured variables. In Refs. 10 and 11, the EKF technique was demonstrated to be reasonable for checking flight data consistency and estimating unmeasured or poorly measured variables. All measured data, after compatibility check, are combined and processed to generate time histories of the aircraft responses to atmospheric disturbance.

III. Compatibility Check and Improved Wind Profile

The EKF technique provides both a check on data consistency and estimates the unmeasured sideslip angle, angular rates, and three-dimensional wind field. At each time instant, the measured flight data are adjusted for biases and measuring noises by satisfying the kinematics relations in airplane flight dynamics among these variables. This process is defined as the compatibility analysis. Figure 1 shows that the bias of each parameter is quite small. In the interval between 30 and 12 s before touchdown, the heading angle was about 41 deg on the average, and the related 05L runway's heading was 53 deg. In the final 12 s, the heading angle was corrected to 50 deg. However, suddenly the heading angle was decreased to 40 deg again. The estimated yaw rate r is shown to have large negative values, and the estimated sideslip angle shows large negative values in the final 4 s and can be traced to the crosswind being from left to right.

The power control (i.e., the tachometer readings) and control surface deflections δ_e, δ_a, δ_r, δ_s, and δ_f are also plotted in Fig. 1. The angles of elevator, stabilizer, and flap are kept roughly at 4, 1, and 30 deg respectively. However, based on the rudder deflection, the pilot appeared to decrab during the period of -10 to -5 s, and then applied the right rudder to try and arrest a negative yaw rate without success. The reduced frequencies k_1 and k_2 (see Fig. 1) are parameters to indicate the degree of unsteadiness or time dependency in unsteady aerodynamics and are estimated in this paper by fitting the local trajectory with a harmonic motion.[6,8] For the longitudinal aerodynamics, the harmonic motion is the one based

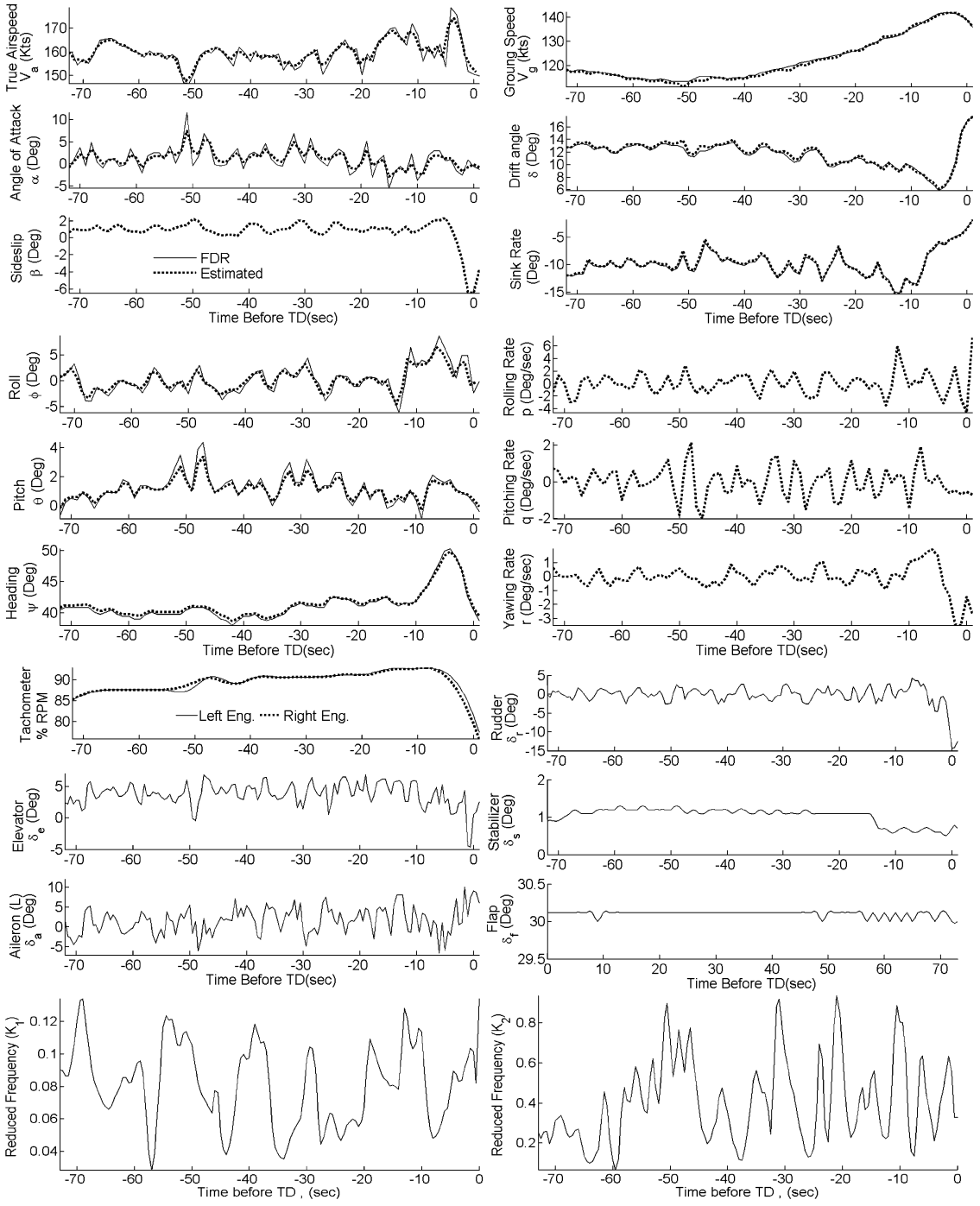

Fig. 1 Time histories of flight data.

on the angle-of-attack variation, whereas for the lateral-directional aerodynamics, it is based on the time variation of roll angle.

The estimated wind field can be expressed in terms of the head wind W_x, crosswind W_y, and vertical wind W_z, respectively. It also can be simplified as the horizontal wind speed V_{w_hor} and wind direction ψ_w. This wind field information can be employed for the purpose of windshear identification. The estimated results can be employed to compare with and verify the recorded wind speed and wind direction (see Table 2).

Because it is important for the safety investigators to have accurate information on the aircraft heights and horizontal positions relative to the runway, the corrected FDR flight data must be verified with an independent source of data. The latter is provided by the global-positioning-system (GPS) data. The accuracy of GPS data is typically in centimeters and should be adequate for the present purpose. Figure 2 shows the flight path before and after the landing. In

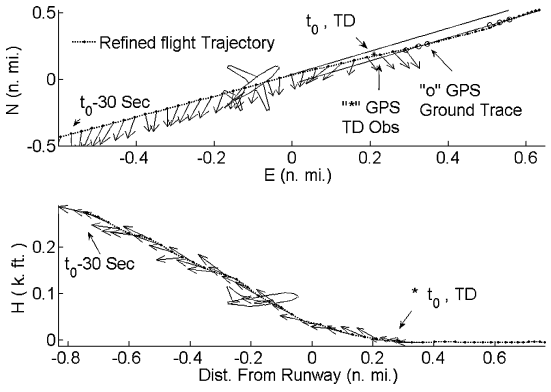

Fig. 2 Flight trajectory with horizontal and vertical wind profiles.

Table 2 Comparisons of wind profiles with FDR readings and EKF estimated results

UTC time, s[a]	FDR WS, kn	Est. WS, kn	FDR WD, deg	Est. WD, deg	Est. W_x, kn	Est. W_y, kn
t_0-60	55	54.2	8.1	8.5	45.2	30.1
t_0-40	51.5	51.1	7	7.3	42.3	28.7
t_0-20	44	44.8	3.5	3.1	36.5	25.6
t_0-8	37.5	37.9	——	3.9	28.6	24.3
t_0-7	——	34.9	5	4.6	26.1	23.1
t_0-6	——	32.0	——	6.0	23.8	21.3
t_0-5	——	29.4	——	7.5	21.7	19.8
t_0-4	27.5	27.3	——	8.5	20.5	18.3
t_0-3	——	26.8	8	8.4	20.4	17.4
t_0-2	——	27.9	——	6.5	21.2	18.0
t_0-1	——	31.1	——	2.0	23.7	20.2
t_0+0	37.0	36.8	——	354.5	25.7	26.6
t_0+1	——	46.0	343	343.1	26.0	38.0
t_0+2	——	——	——	——	——	——
t_0+3	——	——	——	——	——	——
t_0+4	41.5	——	——	——	——	——
t_0+5	——	——	335	——	——	——

[a]The number in parentheses of the UTC Time column represents the reference time before touchdown t_0 presents the touchdown time that was UTC 13:50:12.

Fig. 2, the integrated positions represent the time-integrated results with the corrected discrete FDR data. It clearly illustrates that the corrected FDR data are consistent with the GPS ground track data. The horizontal and vertical wind profiles shown in Fig. 2 along the flight path are helpful to illustrate the flight conditions in a rapidly changing left crosswind near the ground below 200 ft altitude.

Table 2 compares the wind profiles along the flight trajectory from the FDR readings and the EKF estimated results. The estimated wind speed and direction are shown to match rather well with the FDR data. A crosswind component of approximately 26.6 kn was present near the runway. However, this crosswind component was determined to be much higher than the broadcast wind speed. Furthermore, the information on gusty winds with rapid directional change might not have been adequately and accurately provided to the pilot. This judgment is based on the fact that the ground-based anemometers system is not always accurate because the measurements are made at locations other than the relevant landing zone. Typically the air traffic controllers used 2- or 10-min average records for forecasting or oral communication. In other words, the measured wind speed might differ from the actual magnitude at the runway in question and the wind speed (and direction) might be constantly changing.

IV. Wind Effects During Landing

ASC's report[9] indicated that the flight crew disengaged the autopilot at 13:50:03 (9 s before TD), and at that time the localizer and glide-slope information showed that the aircraft position was in a left deviation from the centerline of 05L runway with a 70-ft radar altitude. Under the crosswind condition, a widely adopted operating method, the crab approach, was suggested to maintain wings level at a minimum sideslip angle throughout the approach, flare, and touchdown. On the final flare, the flight crew applied a downwind rudder ($-\delta_r$ with wind blowing from left) to eliminate the crab (i.e., to decrab) and align the airplane with the runway centerline (see Fig. 3). As the rudder was applied, the upwind wing swept forward, thus developing roll. Throughout the touchdown phase upwind aileron application was utilized to keep the wings level. But on slippery runways the crosswind crab angle should be maintained until touchdown. Allowing the airplane to touch down without removing the crab angle would reduce drift toward the downwind side when touching down on wet or icy runways.

To decrab the airplane in crosswind and maintain alignment with the runway during a crosswind landing, the pilot is required to fly the airplane at a sideslip angle. The rudder must be powerful enough to permit the pilot to trim the airplane for the specified crosswinds. FAA requires that a rudder should provide a comfortable minimum

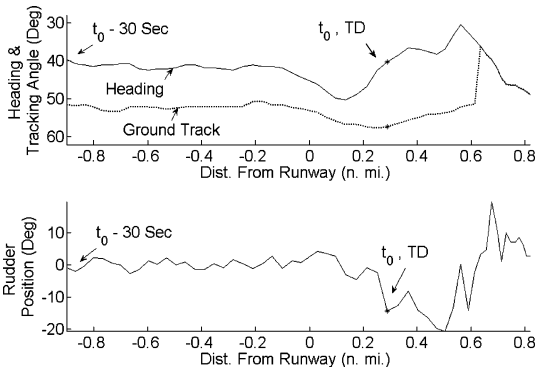

Fig. 3 Time histories of heading, tracking angles, and rudder position.

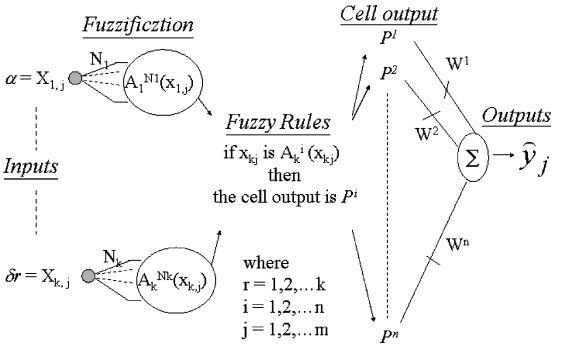

Fig. 4 Schematic of fuzzy-logic modeling.

pedal value at a speed of 150 mph (approximately 240 km/h). The FAA specifications[1] require that the pedal force vary linearly with sideslip β and be constant up to a sideslip angle of ± 15 deg.

The ASC's report indicated that the pilot experienced a loss of lateral-directional control near the ground. That the wind variation caused a hazard or a loss of control cannot be easily verified by the existing parameter identification methods. To analyze the stability and control characteristics of the airplane in the present investigation, a more appropriate method of aerodynamic analysis would be needed. Herein, the refined flight parameters are employed to set up the aerodynamic models through the FLM and FFNN techniques. The FFNN technique is used here mainly to provide an independent check on the FLM results. According to the ASC investigation report, the rain accumulation was around 30 mm in the previous 12 h. The rainfall rate was less than a torrential rainfall rate (over 100 mm/h) in the rain effect studies. Therefore, this study will be focused on wind effects only.

V. Generation of Nonlinear and Unsteady Aerodynamic Models

The general idea of the FLM method describes the relation between its input and the outcome variables and does not require the assumption of functional relationships among influencing state variables and the aerodynamic coefficients. The aerodynamic functional relation is typically unknown. The present modeling method is based on a fuzzy-logic algorithm with internal functions capable of producing continuous aerodynamic derivatives. The schematic of FLM algorithm is presented in Fig. 4 or details, see Refs. 5 and 6. The prediction capability of this method has been demonstrated in Refs. 5, 6, and 8. In this research, the aerodynamic coefficients are assumed in functional forms as

$$C_x, C_N, C_m = y(\alpha, \dot{\alpha}, q, k_1, \beta, \delta_e, M, p, \delta_s, \delta_f, h, \dot{h}) \quad (1)$$

$$C_y, C_l, C_n = y(\alpha, \beta, \phi, p, r, k_2, \delta_a, \delta_r, M, \dot{\alpha}, \dot{\beta}, h, \dot{h}) \quad (2)$$

where C_x, C_N, C_m are the axial-force, normal-force, and pitch-moment coefficients respectively, and C_y, C_l, C_n are the side-force,

rolling- and yawing-moment coefficients. The six aerodynamic coefficients, that is, the outcome variables, can be obtained from the six-degree-of-freedom equations of motion in the body-fixed axes with their origin at the airplane's center of gravity after applying necessary corrections to the measured parameters in a compatibility analysis.[6] The variables on the right-hand sides of Eqs. (1) and (2) are considered as input variables, which are the time histories of refined parameters from the FDR data records.

In Fig. 4, the values of each input variable, such as the angle of attack, are divided into several ranges N_r, each of which represents a membership function having a membership grade equal to $A(X_r)$. In this research, overlapped triangles are the shapes used to represent the fuzziness grades. A fuzzy model is composed of many fuzzy cells that are formed by taking one membership function from each variable. In each fuzzy cell P^i the internal function is assumed to be a linear function of the input parameters.

$$P^i = y_i(x_1, x_2, \ldots, x_r, \ldots, x_k) = p_0^i + \sum_{r=1}^{k} p_r^i x_r \tag{3}$$

where p_0^i and p_r^i are the model coefficients, k is the number of input variables, and $i = 1, 2, \ldots, n$, and n is the total number of fuzzy cells, which is equal to $N_1 \times N_2 \times \cdots N_r \cdots \times N_k$, where N_r is the number of membership functions of the parameter X_r. Then the output of the FLM is the weighted average of all cell outputs, that is,

$$\hat{y}_j = \frac{\sum_{i=1}^{n} W_j^i P^i}{\sum_{i=1}^{n} W_j^i} \tag{4}$$

In Eq. (4), $W_j^i = op[A^i(x_{1,j}), \ldots, A^i(x_{r,j}), \ldots, A^i(x_{k,j})]$ is the weight of the ith cell, and the operator op stands for product operation of its elements, and $j = 1, 2, \ldots, m$, and m is the number of data sets.

There are two main processes involved in the FLM algorithm. One is to identify the best structure of fuzzy cells of the model, that is, to determine the best number of membership functions for each variable. The other is the determination of coefficients of the linear internal functions (i.e., the p_r^i coefficients). The coefficients are calculated with the Newton gradient-descent method by minimizing the sum of squared errors (SSE), and the structure of fuzzy cells is obtained by maximizing the square of multiple correlation coefficients R^2. The SSE and R^2 are defined as

$$\mathrm{SSE} = \sum_{j=1}^{m} (\hat{y}_j - y_j)^2 \tag{5}$$

$$R^2 = 1 - \frac{\left\{\sum_{j=1}^{m} (\hat{y}_j - y_j)^2\right\}}{\left\{\sum_{j=1}^{m} (\bar{y} - y_j)^2\right\}} \tag{6}$$

where $\hat{y}_j$ is the output of the fuzzy-logic model, y_j is the measured data, and $\bar{y}$ is the average value of all data. The resulting aerodynamic models represent the numerical aerodynamic database from which specific aerodynamic characteristics can be extracted. From a statistical point of view, if $R^2 = 0.95$, it implies that 95% of the data are represented and can be explained by the model.

On the other hand, for the present purpose of aerodynamic modeling the FFNN method[7] should also be applicable, although no physical significance can be attached either to the networks structure or to the weights. Theoretically, the FFNNs are composed of groups of neurons that are arranged into an input layer, and the output layer, and one or more hidden layers. The number of nodes (neurons) in the input and output layers are determined, respectively, by the number of input and output variables, whereas the number of neurons in the hidden layer is decided by the complexity of the problem. Each neuron of a layer is connected to each neuron of the next layer, and each connection is assigned its individual connective weight. In the FLM method, the fuzzy cells replace the networks' neurons. Therefore, the FLM method can be considered as a simplified neural-fuzzy method with a single hidden layer.

Table 3 Comparisons of FLM's and FFNN's modeling accuracies[a]

	FLM		FFNN	
Coefficients	R^2	Iterations/ CPU time	R^2	Iterations/ CPU time
C_x	0.9801	20000/15.3 h	0.931	20000/23.0 h
C_m	0.9677	50000/20.0 h	0.957	50000/35.5 h
C_N	0.9712	50000/22.3 h	0.921	50000/38.2 h
C_y	0.9735	20000/16.8 h	0.931	20000/24.2 h
C_l	0.9915	20000/15.2 h	0.945	20000/23.8 h
C_n	0.9715	20000/15.8 h	0.935	20000/24.6 h

[a]CPU time was determined with a CPU 2.4 GHz, RAM 512 Mb, and OS Windows XP laptop.

Table 4 Comparison of FLM's and FFNN's estimated derivatives[a]

Coefficients/ Parameter	FLM			FFNN		
	Case 1	Case 2	Case 3	Case 4	Case 5	Case 6
α, deg	0	5	10	0	5	10
C_m	0.22	−0.03	−0.24	0.18	−0.04	−0.21
$C_{m\alpha}$	−2.865	−2.758	−2.407	−2.521	−2.286	−1.948
C_N	1.13	1.42	1.86	1.16	1.39	1.79
$C_{N\alpha}$	3.323	4.082	5.042	2.636	3.820	4.584
β, deg	0	−5	−10	0	−5	−10
C_y	0.02	0.23	0.48	−0.01	0.25	0.49
$C_{y\beta}$	−2.407	−2.605	−2.865	−2.580	−2.665	−2.750
C_n	0.006	−0.012	−0.008	0.0058	−0.0119	−0.0081
$C_{n\beta}$	0.206	0.075	−0.046	0.203	0.079	−0.044

[a]Control Surface deflections δ_e, δ_s, and δ_f are kept constantly at 4, 1, and 30 deg, respectively. δ_a and δ_r are set to zero.

According to Ref. 7, in FFNNs, the networks structure (the number of neurons), the number of hidden layer, and individual weights are determined by minimizing mean square error (MSE). The criterion for termination of the iterative process in training was based on computed MSE, which is defined as

$$\mathrm{MSE} = \frac{\sum_{j=1}^{m} (\hat{y}_j - y_j)^2}{m} = \frac{\mathrm{SSE}}{m} \tag{7}$$

Results from both the FLM's and FFNN's methods are compared in Table 3. The results indicate that the FLM method can achieve higher R^2 in less amount of computing time than the FFNN technique for the present highly nonlinear data set with multiple varying variables.

Estimated aerodynamic coefficients obtained from the resulting FLM and FFNNs models are presented in Fig. 5. It is observed that the agreement between flight data and the fuzzy model is quite good. Each model involves 20,000 iterations, except the pitching-moment and normal-force coefficients C_m and C_N, which were iterated at each 50,000-iteration interval. In each iteration, the model coefficients in each fuzzy cell are improved and updated. The predicted aerodynamic coefficients are deemed acceptable only if the SSE or MSE is less than a specified value, or R^2 is higher than 0.95 such that the calculated derivatives will not change significantly.

The stability and control derivatives as appeared in the equations of motion of an aircraft represent the partial derivatives of aerodynamic force and moment coefficients with respect to the corresponding motion or control variables. In the present estimation, they are calculated as the changes in the aerodynamic force or moment coefficients as a result of a small variation in one of the motion or control variables about some specified conditions. As one example, assume that only α is perturbed by a small value $\Delta\alpha$, while keeping all other variables unchanged. The predicted values of the pitching-moment coefficients at $\alpha + \Delta\alpha$ and $\alpha - \Delta\alpha$ are C_m^+ and C_m^-, respectively. Then the ratio $(C_m^+ - C_m^-)/2\Delta\alpha$ is the stability derivative $C_{m\alpha}$.

In Table 4, the estimated longitudinal derivatives $C_{m\alpha}$ and $C_{N\alpha}$ are computed with α being 0, 5, and 10 deg, and the perturbation $\Delta\alpha$ as 1 deg. On the other hand, the lateral derivatives $C_{y\beta}$ and $C_{n\beta}$ are computed with β being 0, −5, and −10 deg, and the perturbation $\Delta\beta$ also equals 1 deg. For the present purpose of verifying the

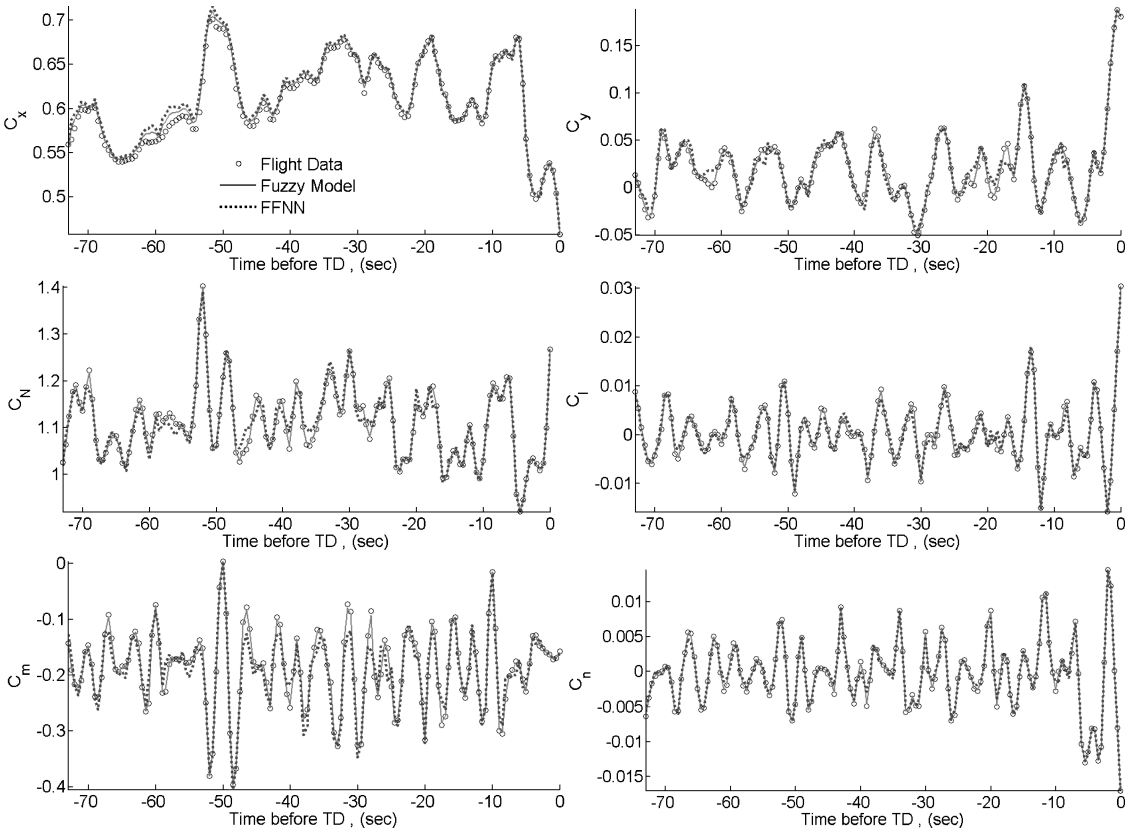

Fig. 5 Comparison of computed and estimate total aerodynamic coefficient.

FLM results, the dynamic parameters $\dot{\alpha}, \dot{\beta}, q, k_1, k_2, p, r, \dot{h}$ are set to zero. Because the rolling-moment and axial-force derivatives are not considered as important in the present investigation, they are not compared. In addition, the damping derivatives are not listed to save time. The control deflections are set to average values in the flight under investigation and indicated in Table 4 as well. The results in Table 4 indicate that the derivatives estimated from FLM or FFNN models are quite similar. It is expected that the damping derivatives should also be comparable. The damping derivatives can be evaluated and compared by using the small-amplitude oscillation method to be described later. Therefore in the following all aerodynamic derivatives will be evaluated only with the FLM models.

VI. Aerodynamic Analysis from FLM Models

A. Stability and Control Effectiveness Derivatives

To evaluate the aerodynamic derivatives along the flight path, perturbations of parameters, one at a time, will be made from the motion time-history values. These derivatives are calculated with the central difference scheme about the instantaneous, not trimmed, flight conditions, and therefore are influenced by dynamic and unsteady aerodynamic effects. The results for the main longitudinal stability and control effectiveness derivatives are presented in Fig. 6. It shows that $C_{N\alpha}$ becomes more positive and $C_{m\alpha}$ more negative near the ground so that an incremental lift and a nose-down pitching moment are induced, consistent with the conventional theory in ground effect, as will be shown in the next section. So far, the longitudinal damping derivatives C_{Nq} and C_{mq} have not been analyzed because the range of exhibited pitch rates in flight was small, that is, the pitching motion was not significantly excited. According to the usual sign convention in the normal situation, $C_{m\delta e}$ should be negative. However, $C_{m\delta e}$ can become positive in some time periods near the ground. This should be interpreted as ineffectiveness of the elevator control in the present dynamic motion, instead of control reversal. This is because when the elevator was deflected up (negative) near the ground, the pitching moment was still increasing negatively, and the elevator was not able to reverse the change. The negatively increasing pitching moment while approaching the

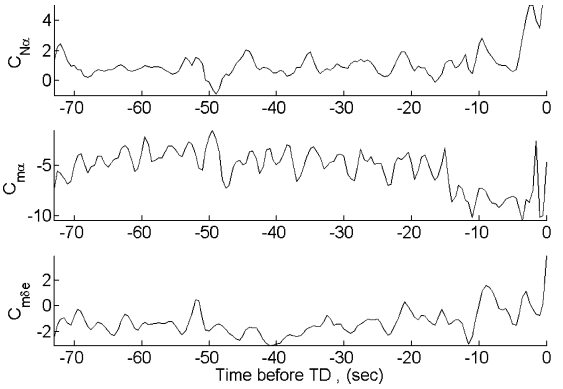

Fig. 6 Longitudinal stability and control effectiveness derivatives.

ground was not caused by the elevator; instead, it was caused by the dynamic ground effect in crosswind. This phenomenon will be discussed later. In Ref. 12 it was shown that when the steady-state flight data for the same airplane were used in modeling, the calculated $C_{m\delta e}$ was a nominal value of -1.106 per radian at $M = 0.35$, $\alpha = 3$ deg, and $\delta_e = 0$ deg.

In the lateral-directional motion (see Fig. 7), the main problem occurred in the directional instability $-C_{n\beta}$, and unstable yaw damping $+C_{\rm nr}$, in particular a few seconds before touchdown. These derivatives are evaluated in the dynamic motion, not about the static trim conditions, but about the instantaneous flight conditions. It is seen that $C_{y\beta}$ tends to be large and negative (the usual sign). However, the fact that a negative value of $C_{y\beta}$ might not correspond to a positive $C_{n\beta}$ at a given time instant can indicate the unsteady aerodynamic effect, similar to the situation between the lift and pitching moment responses in dynamic stall. That is, not only the damping derivatives are affected by the unsteady aerodynamic effect, but the stiffness derivatives $C_{n\beta}$ and $C_{y\beta}$ as well. The magnitude of unsteady aerodynamic effects can also be judged from the hysteresis curves, as will be shown later. These unsteady aerodynamic phenomena make

the aircraft control in sideslip in a strong crosswind much more difficult. In the normal situation, the control derivatives $C_{n\delta r}$ should be negative. As shown in Fig. 7, $C_{n\delta r}$ becomes positive in the final 10 s to make the directional control difficult to achieve. Again, the fact that $C_{n\delta r}$ is positive in a dynamic motion should not be interpreted as control reversal; instead, it is loss of control effectiveness. In fact, it is one of the reasons that the aircraft slipped off the runway after touchdown. As presented in Fig. 1, the roll angle and aileron deflections were maintained within approximately ±5 deg. Therefore, the rolling motion was not regarded as essential in investigating the incident.

The calculated stability and control derivatives in the present dynamic motion tend to vary considerably along the flight path. This phenomenon is caused by the varying motion variables in windshear and the unidentified turbulence and the associated unsteady aerodynamic effects. Again, they are not evaluated at the trim conditions, as is done in a steady-state flight. Instead, they are calculated at the instantaneous flight conditions. Therefore, they are not comparable to those steady-state data used by airplane designers. In regard to an airplane with unstable stability derivatives, even in a steady-state flight flying unstable airplanes with large moments of inertia is still quite possible. As long as the time to double the amplitude is large, pilots can still control the airplane.[13]

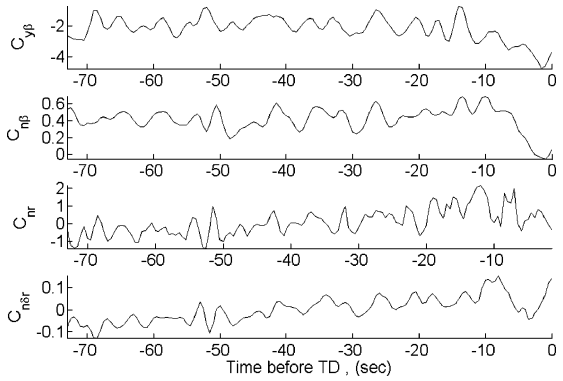

Fig. 7 Lateral stability, damping, and control effectiveness derivatives.

B. Ground-Effect Analysis

In the past, the ground effect in crosswind has not been systematically investigated and analyzed. Most flight data have been acquired without crosswind.[14,15] The present FLM aerodynamic models for the normal-force and pitching-moment coefficients provide data for the analysis of static and dynamic ground effects.[12] In the conventional ground-effect analysis, results are presented at a specified constant angle of attack as functions of the relative ground height h/b, where b stands for the wing span. In the following analysis, there are four cases to be compared: static ground effect ($\dot{h} = 0$), dynamic ground effect ($\dot{h} \neq 0$), and with/without crosswind ($\beta \neq 0$, or $= 0$). In an effort to examine the relative importance of longitudinal stability derivatives, the flight results are extracted from the FLM models by the small-amplitude oscillation method, which are identified with a subscript osc. The reduced frequency is set to $k_1 = 0.05$ along the flight trajectory. For longitudinal aerodynamics, the harmonic motion is the one based on the angle-of-attack variation. Therefore, the time history of α in flight is used as the mean value of oscillatory loop, and the oscillatory amplitude is set to 2.5 deg. The oscillatory amplitude is reduced to 1 deg if α or pitch rate reaches the corresponding assumed range for the variable to avoid extrapolation. The oscillatory longitudinal derivatives are defined as

$$(C_{N\alpha})_{\text{osc}} = C_{N\alpha} - k_1^2 C_{\text{N}\dot{\text{q}}} \tag{8}$$

$$(C_{m\alpha})_{\text{osc}} = C_{m\alpha} - k_1^2 C_{\text{m}\dot{\text{q}}} \tag{9}$$

Figure 8 shows that the sink rates induce higher increments of the normal-force coefficient, but the crosswind tends to produce

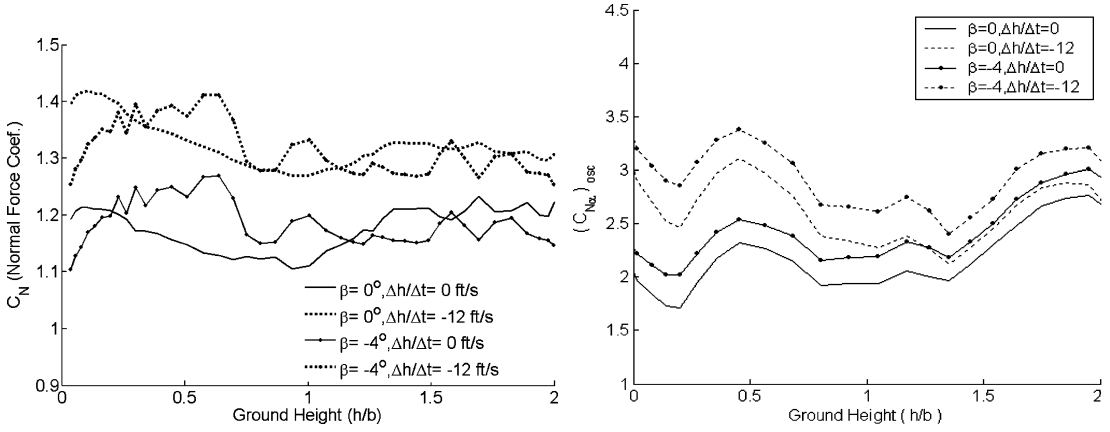

Fig. 8 Variation of normal-force coefficients C_N and longitudinal oscillatory derivatives $(C_{N\alpha})_{\text{osc}}$ in ground effects at $\alpha = 3$ deg.

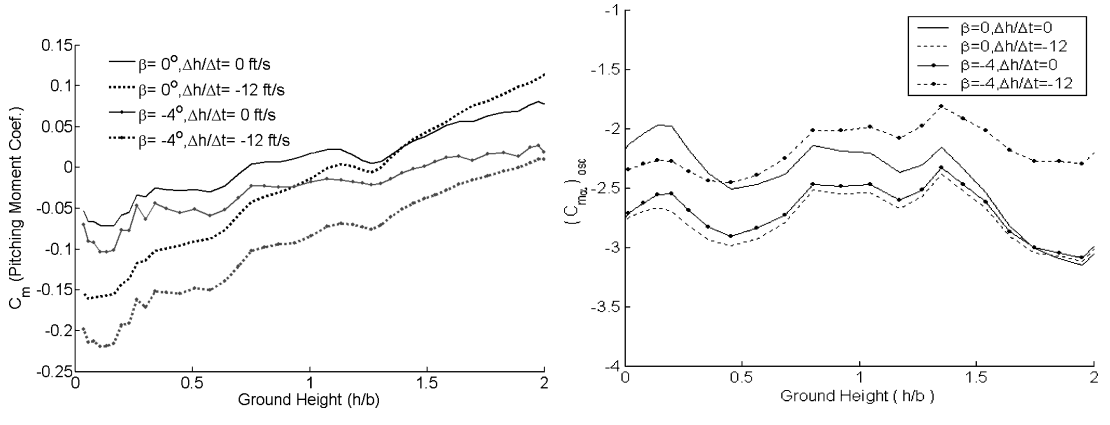

Fig. 9 Variation of pitch-moment coefficients C_m and longitudinal oscillatory derivatives $(C_{m\alpha})_{\text{osc}}$ in ground effects at $\alpha = 3$ deg.

an adverse effect near the ground. The normal-force derivative shows that $(C_{N\alpha})_{\text{osc}}$ is increased by the dynamic ground effect and crosswind.

On the other hand, the effect of ground proximity is to increase the pitch-down tendency. Similarly, sideslip would induce a nose-down pitching moment as well. These tendencies are also exhibited in $C_{m\alpha}$ (see Fig. 9), with the effect of ground proximity producing a more negative $C_{m\alpha}$. It is expected that the contribution of pitch damping derivative to the nose-down moment should be negligible because the pitch rates are generaly small (Fig. 1).

In addition, the crosswind will make the pitching moment more negative. The control effectiveness of the elevator (i.e., $C_{m\delta e}$ being more positive) can also be lost near the ground (see Fig. 10), especially when sideslip is present. The lost of control effectiveness was explained earlier in conjunction with Fig. 6. The probable cause of crosswind inducing adverse dynamic ground effect can be speculated to be that the crosswind induces vortex formation below the wing, such as around the engine nacelles.[16] Reference 16 described a tornado-like vortex developed at the jet engine inlet by crosswind in laboratory experiments. These vortices stay under the main wing because of the dynamic ground effect and produce suck-down pressure on the lower wing surface or nacelles. This phenomenon requires further investigation, preferably by flight testing, to improve safety in aircraft operations. These results can explain the reason for a hard touchdown, exceeding the certified design limits, resulting in a failure of the nose-gear structure of a Tarnsavia Airlines Boeing 757-236 (B757) that landed in strong and gusty crosswind conditions at Schiphol Airport, Amsterdam, Netherlands on 24 Dec. 1997 (Ref. 17).

The unsteady aerodynamic effect caused by varying crosswind during the landing phase can also be verified and illustrated with a hysteresis analysis, as will be shown in the next section.

C. Hysteresis Analysis

Theoretically, the unsteady aerodynamic effect is related to the specific dynamic motion variables, such as α in the longitudinal motions and β or ψ for the lateral or yawing motions. In Ref. 6, hysteresis curves of C_m change the direction only when the reduced frequency is high enough, depending on the flight conditions and aircraft configurations. To demonstrate the $\dot{\beta}$ effect, a pure sideslipping motion is produced, with $\bar{\beta}$ and β_A being the local mean sideslip angle and the amplitude of the harmonic motion, respectively. The hysteresis curves of C_y and C_n are plotted in Fig. 11. Note that the magnitude of damping derivatives depends on the size of hysteresis loops, whereas the stiffness derivatives depend on the slopes of the loops. It is seen that the curves of C_y tend to change from a counterclockwise loop (i.e., $-C_{y\dot{\beta}}$) to a clockwise one (i.e., $+C_{y\dot{\beta}}$) at a high reduced frequency and low sideslip angles. Similarly, the hysteresis curves of C_n show that they can be either in a counterclockwise direction, that is, negative $C_{n\dot{\beta}}$ (or unstable damping), or a clockwise direction, that is, positive $C_{n\dot{\beta}}$ (or stable damping). It indicates that the crosswind disturbance can contribute to dynamic instability in a pure sideslipping motion. Note that the oscillatory yaw damping derivative is defined as

$$(C_{\text{nr}})_{\text{osc}} = C_{\text{nr}} - C_{n\dot{\beta}} \cos\alpha \tag{10}$$

In Fig. 11, unstable damping in yawing motion $+C_{\text{nr}}$ in the flare was also noted. It is most likely that the lateral upset and unstable flight is caused by the rapid change of crosswind.

D. Windshear Hazards

A useful parameter adopted by FAA[2] and often quoted for indicating the severity of windshear and vertical wind on the aircraft performance is the F factor:

$$F \approx \frac{\dot{W}_x}{g} + \frac{W_z}{V_a} \tag{11}$$

$$\bar{F} = \frac{1}{L}\int_x^{x+L} F\,\mathrm{d}s \tag{12}$$

where $\dot{W}_x$ is the rate of change of the horizontal wind component along the aircraft flight path, g is the acceleration due to gravity, and V_a the airspeed of the aircraft. The first term on the right-hand side of Eq. (11) represents the contribution caused by the headwind change, whereas the second term represents the contribution caused by the vertical wind. FAA has adopted 1-km (=L) averaged F-factor index $\bar{F}$ to represent a persisted deterioration of hazardous conditions. In addition, a threshold of $\bar{F} = 0.13$ has been adopted. Figure 12 indicates the characteristics of the estimated headwind being decreasing when the aircraft was near the ground. On the other hand, the estimated crosswind was constant for most of the time until the final 10 s. It can be seen that the averaged F factor $\bar{F}$ is not over 0.13. Yet the aircraft did have problem in control. The windshear identification results show that these methods are not adequate when the wind speed and/or direction vary rapidly. Therefore, the present aerodynamic analysis can significantly improve the investigation of incidents or accidents in dynamic flight conditions by providing additional information on airplane's stability and control characteristics.

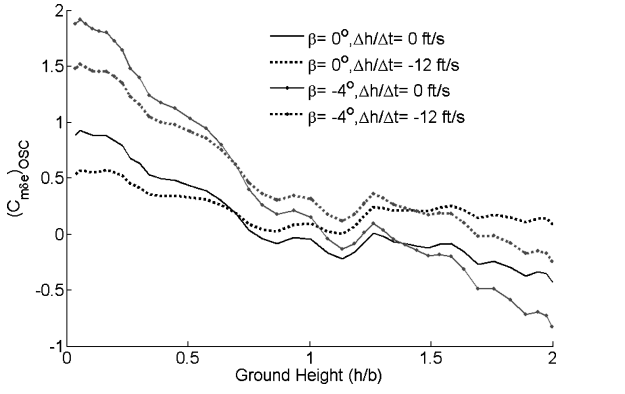

Fig. 10 Longitudinal control effectiveness $C_{m\delta e}$ in ground effects at $\alpha = 3$ deg.

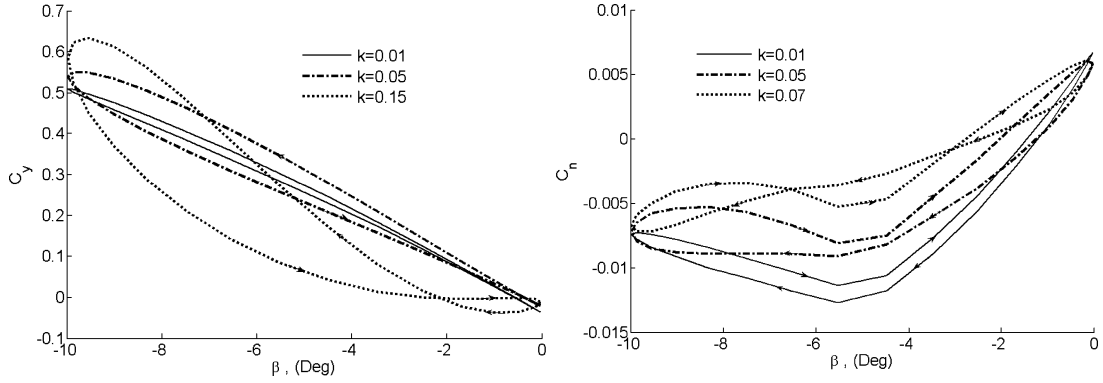

Fig. 11 Effects of reduced frequency on C_y and C_n ($\bar{\beta} = -5$ deg and $\beta_A = 5$ deg in each harmonic loop).

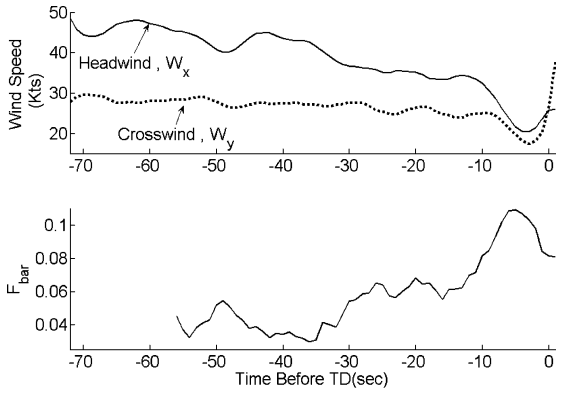

Fig. 12 Time histories of estimated W_x, W_y, $\bar{F}$.

VII. Conclusions

This paper focused on the estimation of windshear effects on flight dynamics from the viewpoint of aerodynamic stability and control effectiveness. Based on one set of flight-data-recorder data from a jet transport airplane involved in an incident in landing during windshear encounter, unsteady aerodynamic models were established with a fuzzy-logic algorithm. The analysis with these aerodynamic models indicated that directional instability and loss of yaw control effectiveness contributed to the incident. The aerodynamic instability, in turn, was caused in part by the unsteady aerodynamic effects in the varying crosswind. Dynamic ground effect in crosswind would also increase the adverse effect. To improve flight safety, windshear guidelines should be improved by accounting for possible directional instability and loss of rudder effectiveness near the ground in a combined crab and sideslip landing.

References

[1]"AC 00-54 Subject: Pilot Windshear Guide," AC 00-54, Federal Aviation Administration, Washington, DC, Nov. 1985.

[2]"Windshear Training Aid, Example Windshear Training Program," AVA 19756-KK00, Federal Aviation Administration, Washington, DC, Nov. 1986.

[3]"Wind Shear," ICAO Circular 186-AN/122, International Civil Aviation Organization, Montreal, 1987.

[4]Weng, C. T., Ho, C. S., and Lan, C. E., "Building a Nonlinear Unsteady Aerodynamic Model for a Windshear Related Jet Transport," *Transactions of the Aeronautical Society of the Republic of China*, Vol. 36, No. 3, 2004, pp. 215–224.

[5]Wang, Z., Lan, C. E., and Brandon, J. M., "Fuzzy Logic Modeling of Nonlinear Unsteady Aerodynamics," AIAA Paper 98-4351, Aug. 1998.

[6]Weng, C.-T., Lan, C. E., and Ho, C.-S., "Aerodynamic Model Estimation and Analysis for a Jet Transport in a Landing Accident," AIAA Paper 2003-5699, Aug. 2003.

[7]Ghosh, A. K., and Khubchandan, S., "Estimation of Aircraft Lateral-Directional Parameters Using Neural Networks," *Journal of Aircraft*, Vol. 35, No. 6, 1998, pp. 876–881.

[8]Pan, C. C., and Lan, C. E., "Estimation of Aerodynamic Characteristics of a Jet Transport Using Accident FDR Data," AIAA Paper 2002-4494, Aug. 2002.

[9]"Mandarin Airline Flight AE838 Boeing 737-809, CKS Airport," Aviation Safety Council, Taipei Aircraft Serious Incident Rept., Nov. 2001.

[10]Klein, V., and Schiess, J. R., "Compatibility Check of Measured Aircraft Responses Using Kinematics Equations and Extend Kalman Filter," NASA TN D-8514, Aug. 1977.

[11]Weng, C.-T., and Ho, C.-S., "Unsteady Aerodynamic Analysis Under Wind Shear Effect by EKF Method on FDR Data," *Proceedings of Institute of Navigation 2004 National Technical Meeting*, Jan. 2004, pp. 897–902.

[12]Weng, C.-T., Lan, C. E., and Ho, C.-S., "Analysis of Dynamic Ground Effect for a Jet Transport in Crosswind," AIAA Paper 2004-5066, Aug. 2004.

[13]Roskam, J., *Airplane Flight Dynamics and Automatic Flight Controls, Part I*, DAR Corp., Lawrence, KS, Jan. 2001, p. 192.

[14]Curry, R. E., and Bowers, A. H., "Ground Effect Analysis of a Jet Transport Airplane," NASA TM-85920, Jan. 1985.

[15]Corda, S., Stephenson, M. T., Burcham, F. W., and Curry, R. E., "Dynamic Ground Effects Flight Test of an F-15 Aircraft," NASA TM-4604, Sept. 1994.

[16]Eagleman, J. R., Muirhead, V. U., and Willems, N., "Thunderstorms, Tornadoes and Damage to Building," Univ. of Kansas, Final Research Report to Grant #EC00303, Environment Control Administration, Dept. of Health, Education, and Welfare, LC number: QC955.E333, Lawrence, KS, Dec. 1971, p. 90.

[17]"Crew Fails to Compute Crosswind Component, Boeing 757 Nosewheel Collapses on Landing," *Flight Safety Foundation, Accident Prevention*, Vol. 57, No. 3, March 2000, pp. 1–8.